Proc. Natl. Acad. Sci. USA
Vol. 92, pp. 10949–10953, November 1995
Physiology

Structure determination of murine mitochondrial carbonic anhydrase V at 2.45-Å resolution: Implications for catalytic proton transfer and inhibitor design

(protein crystallography/enzymology/zinc enzyme/carbon dioxide hydration)

P. ANN BORIACK-SJODIN*, ROBERT W. HECK†, PHILIP J. LAIPIS†, DAVID N. SILVERMAN‡, AND DAVID W. CHRISTIANSON*§

*Department of Chemistry, University of Pennsylvania, Philadelphia, PA 19104-6323; and †Department of Biochemistry and Molecular Biology, and ‡Department of Pharmacology and Therapeutics, University of Florida College of Medicine, Gainesville, FL 32610-0267

Communicated by Robert E. Forster II, University of Pennsylvania School of Medicine, Philadelphia, PA, August 14, 1995 (received for review February 15, 1995)

ABSTRACT **The three-dimensional structure of murine mitochondrial carbonic anhydrase V has been determined and refined at 2.45-Å resolution (crystallographic *R* factor = 0.187). Significant structural differences unique to the active site of carbonic anhydrase V are responsible for differences in the mechanism of catalytic proton transfer as compared with other carbonic anhydrase isozymes. In the prototypical isozyme, carbonic anhydrase II, catalytic proton transfer occurs via the shuttle group His-64; carbonic anhydrase V has Tyr-64, which is not an efficient proton shuttle due in part to the bulky adjacent side chain of Phe-65. Based on analysis of the structure of carbonic anhydrase V, we speculate that Tyr-131 may participate in proton transfer due to its proximity to zinc-bound solvent, its solvent accessibility, and its electrostatic environment in the protein structure. Finally, the design of isozyme-specific inhibitors is discussed in view of the complex between carbonic anhydrase V and acetazolamide, a transition-state analogue. Such inhibitors may be physiologically important in the regulation of blood glucose levels.**

The carbonic anhydrase (CA; EC 4.2.1.1) family of zinc metalloenzymes consists of seven known isozymes which catalyze the hydration of carbon dioxide to yield bicarbonate ion and a proton (1–3). Located in the alkaline environment of the mitochondrial matrix (4–8), CA-V is unique among the family of mammalian carbonic anhydrases because it is the only isozyme known to be compartmentalized in a cellular organelle. Since the inner mitochondrial membrane is impermeable to bicarbonate (9), CA-V ensures a constant supply of bicarbonate in the mitochondrial matrix for the generation of carbamoyl phosphate in the urea cycle and the conversion of pyruvate into oxaloacetate in gluconeogenesis (10, 11). With $k_{cat}/K_m = 3 \times 10^7\ M^{-1}\cdot s^{-1}$ (12), the activity of CA-V is intermediate between that of CA-II ($k_{cat}/K_m = 1.5 \times 10^8\ M^{-1}\cdot s^{-1}$) (13) and CA-III ($k_{cat}/K_m = 3 \times 10^5\ M^{-1}\cdot s^{-1}$) (14) and is comparable to that of CA-I ($k_{cat}/K_m = 5 \times 10^7\ M^{-1}\cdot s^{-1}$) (13).

Isozyme CA-V is also unique among the CAs due to the location of a catalytic proton-shuttle group which transfers the product proton from zinc-bound water to buffer. In CA-II, the most studied isozyme, this residue is His-64 (15, 16). CA-V has Tyr-64 (17), which is consistent with the pK_a of 9.2 found for the proton acceptor, but initial mutagenesis studies suggest that this residue is not the major proton shuttle (12). Therefore, the evolution of catalytic proton-shuttle groups in CA isozymes appears to have diverged. To further illustrate the comparison, His-200 is the best candidate for a proton shuttle in CA-I because of its proximity to the zinc ion and its pK_a (18). In CA-III there appears to be no proton-shuttle residue in the active site, and the product proton is probably transferred directly to bulk solvent (14, 19). Finally, inspection of the deduced amino acid sequences of CA-IV, CA-VI, and CA-VII reveals a histidine at position 64 (20). Different proton shuttle residues contribute to the range of k_{cat} values (10^3–$10^6\ s^{-1}$) measured for different CA isozymes, and knowledge of the three-dimensional structure of each isozyme is a prerequisite to understanding these kinetic differences. With regard to CA-V, the question remains: Where is the catalytic proton shuttle?

To answer this question and to clarify structure–activity relationships within the greater family of carbonic anhydrases, we report the x-ray crystallographic structure determinations of murine CA-V and its acetazolamide complex at 2.45-Å resolution.¶ In particular, we have crystallized a deletion variant of CA-V lacking the N-terminal 21 residues due to its stability against proteolysis; however, this deletion does not affect the catalytic activity (12). Kinetic studies (12) interpreted in light of these structures allow for detailed structural inferences on the catalytic mechanism. Additionally, significant insight is gained on design strategies for isozyme-specific CA inhibitors.

MATERIALS AND METHODS

An N-terminally truncated form of murine CA-V was overexpressed in *Escherichia coli* and purified as described (12). Two cDNA clones obtained from independent reverse transcription–PCR of BALB/c liver mRNA were sequenced; differences from published data (8, 17) were confirmed by using BALB/c genomic DNA (R.W.H., R. Manda, and P.J.L., unpublished results). Purified protein was crystallized at pH 7.0 by precipitation against polyethylene glycol 8000. Initial x-ray diffraction data to 2.8-Å resolution were collected with an R-AXIS IIc image plate detector mounted on an RU-200HB rotating-anode generator with double focusing mirrors operating at 50 kV and 100 mA. Data were collected in successive 25-min 2° oscillations about ϕ for a total scan of 180°; the crystal-to-detector distance was set at 100 mm. The crystal orientation was established with REFIX (21) and data were reduced with MOSFLM (22).

Crystals of CA-V belong to triclinic space group *P*1 with unit cell parameters $a = 48.7$ Å, $b = 60.4$ Å, $c = 60.4$ Å, $\alpha = 67.7°$, $\beta = 75.3°$, and $\gamma = 75.2°$ (two molecules in the unit cell).

The publication costs of this article were defrayed in part by page charge payment. This article must therefore be hereby marked "*advertisement*" in accordance with 18 U.S.C. §1734 solely to indicate this fact.

Abbreviation: CA, carbonic anhydrase.

§To whom reprint requests should be addressed.

¶The atomic coordinates have been deposited in the Protein Data Bank, Chemistry Department, Brookhaven National Laboratory, Upton, NY 11973 (reference 1DMZ and 1DMY).

Alternatively, diffraction data could be indexed in monoclinic space group $C2$ with unit cell parameters $a = 100.3$ Å, $b = 67.4$ Å, $c = 48.65$ Å, and $\beta = 107.8°$ (one molecule in the asymmetric unit), but we continued the structure determination in the triclinic system.

Initial phases for the electron density map of CA-V were obtained by molecular replacement using AMORE (23) as implemented in CCP4 (24). The atomic coordinates of human CA-II refined to 1.54-Å resolution (25) were obtained from the Brookhaven Protein Data Bank (26) and modified so that nonidentical residues with CA-V were truncated to alanine or glycine; the modified molecule was used as a search probe in rotation and translation functions. The two highest peaks in the cross-rotation function were at 13.7 σ and 13.1 σ ($\alpha = 336.50°$, $\beta = 41.29°$, $\gamma = 111.07°$ and $\alpha = 225.79°$, $\beta = 59.84°$, $\gamma = 17.26°$, respectively), corresponding to the two molecules in the unit cell. Subsequent translation searches yielded 12.2 σ and 10.5 σ solutions at the origin and at $T_x = 0.6505$, $T_y = 0.6524$, and $T_z = 0.6550$. Rigid-body refinement of the two independent CA-V molecules lowered the crystallographic R factor from 0.38 to 0.36.

Refinement of the structure was performed with XPLOR (27), and model building was performed with CHAIN (28) installed on a Silicon Graphics Indigo workstation. Both molecules in the unit cell were refined without noncrystallographic symmetry constraints, and thermal B factors were initially fixed at 15 Å^2. Simulated annealing refinement (29) was performed after the entire CA-V sequence (8, 17) (R.W.H., R. Manda, and P.J.L., unpublished results) was properly registered in both molecules in the unit cell. B-factor refinement commenced when the R factor dropped to 0.22, and water molecules were added when the crystallographic R factor dropped below 0.20. Additionally, data to 2.45-Å resolution were collected and included in the final rounds of refinement. The final crystallographic R factor for data between 6.5- and 2.45-Å resolution is 0.187 [$R_{free} = 0.294$ (30)], with excellent stereochemistry and 134 water molecules; pertinent data collection and refinement statistics are reported in Table 1.

Table 1. Data collection and refinement statistics for murine CA-V

	Native enzyme	Acetazolamide complex
No. of crystals	1	1
No. of measured reflections	43,483	43,694
No. of unique reflections	21,757	21,632
Maximum resolution, Å	2.45	2.45
Completeness of data, %	98	98
R_{sym}*	0.081	0.073
No. of water molecules in final cycle of refinement	134	104
No. of reflections used in refinement (6.5–2.45 Å)	20,322	20,266
Crystallographic R factor†	0.187	0.185
Free R factor‡	0.294	—
rms deviation from ideal		
Bond lengths, Å	0.011	0.011
Bond angles, degrees	1.8	1.8
Dihedral angles, degrees	26.1	26.1
Improper dihedral angles, degrees	1.4	1.4

*R_{sym} for replicate reflections, $R = \Sigma|I_{hi} - \langle I_h\rangle|/\Sigma\langle I_h\rangle$; I_{hi} = intensity measured for reflection h in data set i; $\langle I_h\rangle$ = average intensity for reflection h calculated from replicate data.
†Crystallographic R factor, $R = \Sigma||F_o| - |F_c||/\Sigma|F_o|$; $|F_o|$ and $|F_c|$ are the observed and calculated structure factors, respectively.
‡Ref. 30.

RESULTS AND DISCUSSION

Structure of Murine CA-V. The amino acid sequence of CA-V registered in the electron density map differs by five amino acids from the sequence originally reported (17). Correction of an apparent sequencing error results in the replacement of Phe-121–Met-122 by Val-121–His-122–Trp-123; this change, which restores sequence similarities with other carbonic anhydrases, was reported by Nagao and colleagues (8). In addition, Leu-185 and Thr-225 are replaced by methionine residues. These methionines presumably result from sequence polymorphisms between C57BL/10 and C57BL/6 mice (8, 17) and the BALB/c-derived clone used here (R.W.H., R. Manda, and P.J.L., unpublished results). The CA-V deletion variant studied here is identical to one purified from mouse liver (R.W.H., C. K. Tu, and P.J.L., unpublished results), and it has full enzymatic activity (12). It behaves similarly to enzyme fractions isolated from guinea pig liver (31) and COS cells (8).

The structures of both molecules of CA-V in the unit cell are refined with excellent backbone conformations: out of 468 total residues, only Arg-252 of molecule B exhibits a disallowed conformation, due to ambiguous main-chain density. Three residues at the N terminus (Ser-22 to Glu-24) and eight residues at the C terminus (Leu-262 to Ser-269) lack well-defined electron density, and these residues are omitted from the final model. A rms deviation of 0.29 Å is calculated for backbone atoms in the least-squares superposition of the two independently refined molecules of CA-V in the unit cell, and most significant differences are confined to segments at the protein surface. This is consistent with the rms coordinate error of 0.32 Å calculated with relationships derived by Luzzati (32).

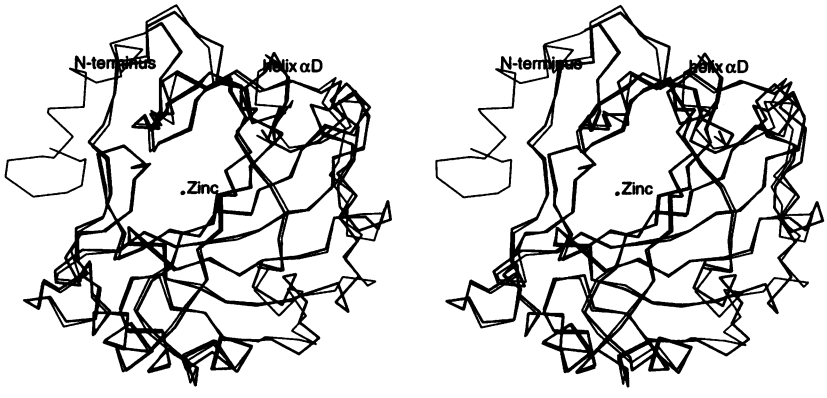

FIG. 1. Least-squares superposition of C^α atoms of murine CA-V (thick bonds) and human CA-II (thin bonds). The N terminus, helix αD, and zinc are indicated.

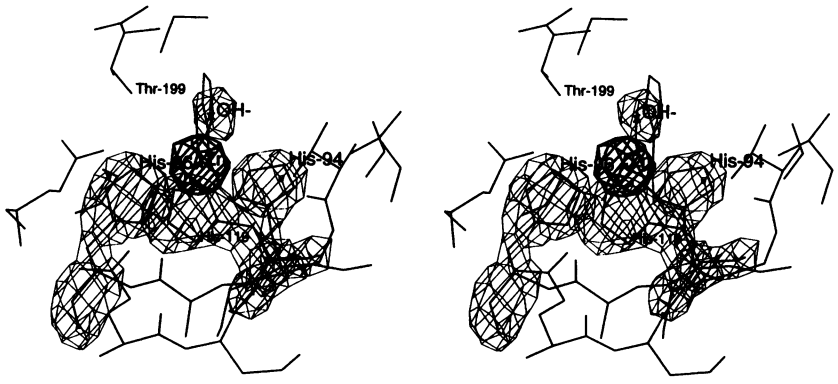

FIG. 2. CA-V active site: difference electron density map calculated with Fourier coefficients $|F_o|-|F_c|$ and phases derived from the final model less the zinc ligands, contoured at 5.0 σ (thin lines); difference electron density map calculated with Fourier coefficients $|F_o|-|F_c|$ and phases derived from the final model less the zinc ion, contoured at 12 σ (thick lines). Refined atomic coordinates are superimposed.

In the prototypical isozyme, CA-II, the first 21 residues comprise a small, partly α-helical segment on the surface of the enzyme adjacent to the active site. However, the deletion of these residues in CA-V affects neither the activity (12) nor the structure of the protein core (Fig. 1). The least-squares superposition of human CA-II and murine CA-V (52% sequence identity for residues 22–261) yields a rms deviation for backbone atoms of 0.93 Å, which is consistent with the expected value of 0.9 Å (33). However, important segmental differences are apparent, the most functionally significant of which is the insertion Ser-125 in the sequence of CA-V relative to CA-II. This insertion extends a loop connecting strand βE to helix αD, and helix αD in turn shifts $\approx$2 Å toward the zinc (Fig. 1).

The zinc coordination polyhedron is conserved between CA-V and CA-II (Fig. 2), as are hydrogen bond interactions between the zinc ligands and their protein environment (i.e., the Thr-199–zinc-bound hydroxide, Gln-92–His-94, Asn-244–His-96, and Glu-117–His-119 hydrogen bonds). Such indirect protein–metal interactions are important for the stability and function of the bound metal ion (34). Additionally, the hydrophobic wall and substrate association pocket (35–38) are conserved with the exception of one key amino acid substitution: Phe-131 of CA-II appears as Tyr-131 in CA-V, where its phenolic side chain accepts a hydrogen bond from the side-chain carboxamide NH_2 group of Gln-92. Significantly, Tyr-131 is located on helix αD and is directed toward the active site. This seemingly conservative amino acid substitution, plus the segmental shift of helix αD, has substantial implications for catalytic proton transfer. Finally, striking active-site differences are also found in the region of residue 64. In CA-II, the sequence flanking this residue is Gly-63–His-64–Ala-65, whereas in CA-V the corresponding sequence is Gly-63–Tyr-64–Phe-65. The conformation of Tyr-64 in CA-V contrasts with that of His-64 in CA-II because Tyr-64 must avoid a steric clash with the adjacent, bulky side chain of Phe-65 (Fig. 3).

Structural Aspects of Proton Transfer in Catalysis. The diminished k_{cat} value for carbon dioxide hydration by CA-V relative to that measured for CA-II suggests that differences in the location and identity of a catalytic proton-shuttle group of $pK_a \approx 9$ and/or solvent structure in the enzyme active site is responsible for kinetic differences (12). Although His-64 is the catalytic proton shuttle of CA-II (15, 16), site-directed mutagenesis studies suggest that Tyr-64 is not the major proton shuttle of CA-V: Tyr-64 $\rightarrow$ His CA-V is no more active in carbon dioxide hydration than wild-type CA-V (12), and Tyr-64 $\rightarrow$ Ala CA-V is nearly as active as the wild-type enzyme (R.W.H., P.J.L., and D.N.S., unpublished results). Moreover, a catalytic role for CA-V residue 64 in proton transfer is probably compromised due to the adjacent bulky side chain of Phe-65. This residue may hinder the formation of an effective solvent bridge between zinc-bound water and residue 64, just as it does in Ala-65 $\rightarrow$ Phe CA-II (L. Scolnick and D.W.C., unpublished results): bulky residues substituted for Ala-65 in CA-II decrease k_{cat}, apparently hindering proton transfer between zinc-bound solvent and His-64 (J. E. Jackman, C.-C. Huang, and C. A. Fierke, personal communication).

The elimination of Tyr-64 as the major proton shuttle in CA-V leaves us with an important question: Is there another catalytic proton shuttle? To address this question, we can

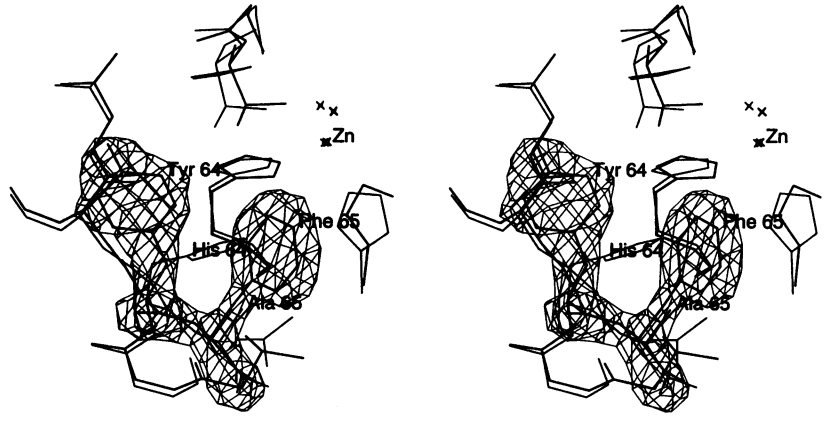

FIG. 3. Difference electron density map of the residue 64 region of CA-V calculated with Fourier coefficients $|F_o|-|F_c|$ and phases derived from the final model less Tyr-64 and Phe-65, contoured at 4.0 σ. Atomic coordinates of the least-squares superposition of CA-V (thick lines) and CA-II (thin lines) are shown; Tyr-64 and Phe-65 (CA-V) and His-64 and Ala-65 (CA-II) are indicated. Zinc-bound solvent appears as an asterisk.

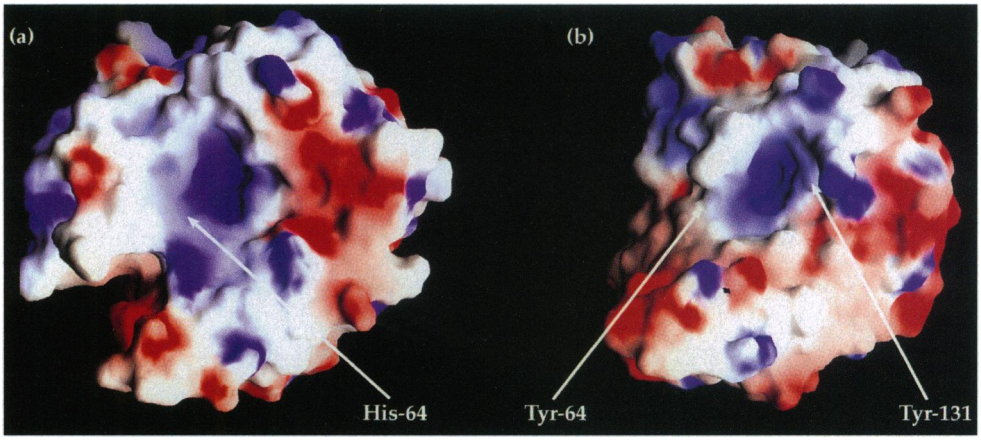

FIG. 4. Electrostatic surface potential of human CA-II (*a*) and murine CA-V (*b*) calculated with GRASP (39); the color scale ranges from −8 kT (red) to +8 kT (blue). Orientation is the same as in Fig. 1. Tyr-64 and Tyr-131 of CA-V and His-64 of CA-II are indicated.

speculate on possible proton shuttle residues by examining the active-site structure and identifying residues that fit the following criteria (as exemplified by His-64 of CA-II): (*i*) the residue must be a reasonable distance from zinc-bound hydroxide (≤10 Å), (*ii*) the residue must be solvent accessible (≥85 Å^2), and (*iii*) the pK_a of the residue must not differ substantially from the pH of the biological environment in which the enzyme functions.

Inspection of the CA-V structure reveals that Tyr-131 apparently satisfies these three criteria optimally. The phenolic hydroxyl group of Tyr-131 is 8.0 Å from zinc-bound solvent and the side chain exposes 103 Å^2 of solvent-accessible surface area. The pK_a of a tyrosine side chain is fairly high (≈10); however, Tyr-131 resides in an electropositive region of the protein surface, in close proximity to three positively charged lysine residues: 91, 132, and 133. This may depress the pK_a of Tyr-131 closer to the alkaline pH of the mitochondrial matrix, and closer to the inferred pK_a of 9.2 for the catalytic proton shuttle (12). Moreover, the electrostatic surface potential of Tyr-131 in CA-V is comparable to that His-64 in CA-II (Fig. 4). Therefore, the location, the electrostatic surface potential, and the solvent accessibility of Tyr-131 should facilitate a possible role in proton transfer. Despite its disorder in electron density maps, the adjacent residue Lys-132 might be an additional candidate. Hydrogen-bonded solvent molecules in the active site will provide additional clues regarding possible proton transfer routes; we await the collection of higher-resolution diffraction data in order to fully define such solvent structure. Of course, until further experiments are performed it is possible that Tyr-131 is not the (sole) catalytic proton shuttle in CA-V; if so, the structural criteria outlined in the previous paragraph will be revised accordingly.

Structural and Physiological Consequences of Inhibitor Binding. Given the immediate active-site similarities of CA-II and CA-V within a 5- to 8-Å radius of zinc, it is not surprising that the affinity of the transition-state analogue acetazolamide is identical to both isozymes (12). In order to probe the structural basis of inhibitor recognition by CA-V, crystals of the CA-V–acetazolamide complex were prepared. X-ray data acquisition and structure refinement statistics are reported in Table 1, and a difference electron density map (Fig. 5) reveals an acetazolamide binding mode of CA-V that is similar, but not identical, to that of CA-II (40). The ionized sulfonamide nitrogen of the inhibitor displaces the zinc-bound hydroxide ion of the native enzyme and simultaneously donates a hydrogen bond to the hydroxyl group of Thr-199; additionally, numerous van der Waals contacts are made with active-site residues. Differences in acetazolamide binding to each isozyme occur in the vicinity of residue 131—i.e., where the three-dimensional structures of each active-site cleft begin to diverge, about 8 Å away from zinc-bound solvent. The carbonyl of the inhibitor hydrogen bonds with the hydroxyl group of Tyr-131 in CA-V, a contact not possible with Phe-131 of CA-II.

For inhibitors that would interact more extensively with the nonconserved Tyr-131 or Tyr-64 regions of the enzyme active site, we predict that differing isozyme specificities may be achieved. For example, inhibitors which discriminate between human CA isozymes I and II have been synthesized by combinatorial methods (41), and acetazolamide itself exhibits differing affinities toward isozymes II and IV (42). Isozyme-inhibitor discrimination requires divergent structural features in each CA active site: in the CA-V active site, the Tyr-131 and Tyr-64 regions represent such features that can be exploited in future inhibitor design experiments.

Inhibitors specific for CA-V may be pharmaceutically important as hypoglycemic agents, given that this isozyme provides bicarbonate ion for the first step of gluconeogenesis. Studies of rat liver mitochondria confirm the requirement of matrix CA for net carbon dioxide uptake (43), so it is not surprising that the nonspecific CA inhibitor acetazolamide lowers glucose levels in perfused rat kidney (44). Additionally, the nonspecific CA inhibitor ethoxzolamide reduces the production of glucose in guinea pig hepatocytes (10) and in rat renal proximal tubules (45). Thus, an inhibitor specific for CA-V might likewise reduce blood glucose levels without

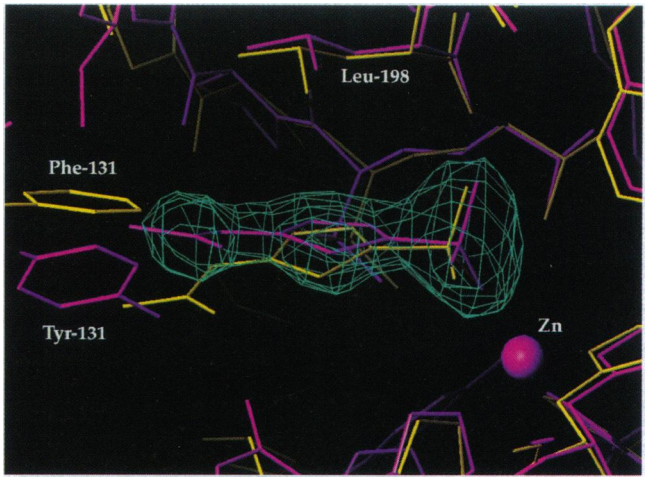

FIG. 5. Difference electron density map of the CA-V–acetazolamide complex calculated with Fourier coefficients $|F_o| - |F_c|$ and phases derived from the final model less the inhibitor, contoured at 4.5 σ. Atomic coordinates of the least-squares superposition of the CA-V–acetazolamide complex (purple) and the CA-II–acetazolamide complex (yellow) are shown.

resulting in side effects that accompany systemic dosing with nonspecific CA inhibitors. The structure of acetazolamine-complexed CA-V will therefore serve as an important foundation for the structure-assisted design of isozyme-specific inhibitors.

We thank Drs. Brian McKeever and James Springer for the atomic coordinates of the CA-II–acetazolamide complex. We thank Dr. Susan M. Tanhauser for the initial cDNA and expression clones and many helpful discussions. Finally, we thank the National Institutes of Health for Grants GM45614 (to D.W.C.) and GM25154 (to D.N.S. and P.J.L.).

1. Silverman, D. N. & Lindskog, S. (1988) *Acc. Chem. Res.* **21,** 30–36.
2. Botré, F., Gros, G. & Storey, B. T., eds. (1991) *Carbonic Anhydrase: From Biochemistry and Genetics to Physiology and Clinical Medicine* (VCH, Weinheim).
3. Dodgson, S. J., Tashian, R. E., Gros, G. & Carter, N. D., eds. (1991) *The Carbonic Anhydrases: Cellular Physiology and Molecular Genetics* (Plenum, New York).
4. Datta, P. K. & Shepard, T. H. (1959) *Arch. Biochem. Biophys.* **81,** 124–129.
5. Maren, T. H. & Ellison, A. C. (1967) *Mol. Pharmacol.* **3,** 503–508.
6. Dodgson, S. J., Forster, R. E., Storey, B. T. & Mela, L. (1980) *Proc. Natl. Acad. Sci. USA* **77,** 5562–5566.
7. Nagao, Y., Platero, J. S., Waheed, A. & Sly, W. S. (1993) *Proc. Natl. Acad. Sci. USA* **90,** 7623–7627.
8. Nagao, Y., Srinivasan, M., Platero, S. J., Svendrowski, M., Waheed, A. & Sly, W. S. (1994) *Proc. Natl. Acad. Sci. USA* **91,** 10330–10334.
9. Chappell, J. B. & Crofts, A. R. (1966) in *Regulation of Metabolic Processes in Mitochondria*, eds. Tager, J. M., Papa, S., Quagliariello, E. & Slater, E. C. (Elsevier, Amsterdam), pp. 293–314.
10. Dodgson, S. J. & Forster, R. E. (1986) *Arch. Biochem. Biophys.* **251,** 198–204.
11. Dodgson, S. J. & Forster, R. E. (1986) *J. Appl. Physiol.* **60,** 646–652.
12. Heck, R. W., Tanhauser, S. M., Manda, R., Tu, C. K., Laipis, P. J. & Silverman, D. N. (1994) *J. Biol. Chem.* **269,** 24742–24746.
13. Khalifah, R. G. (1971) *J. Biol. Chem.* **246,** 2561–2573.
14. Jewell, D. A., Tu, C. K., Paranawithana, S. R., Tanhauser, S. M., LoGrasso, P. V. Laipis, P. J. & Silverman, D. N. (1991) *Biochemistry* **30,** 1484–1490.
15. Steiner, H., Jonsson, B.-H. & Lindskog, S. (1975) *Eur. J. Biochem.* **59,** 253–259.
16. Tu, C., Silverman, D. N., Forsman, C., Jonsson, B. H. & Lindskog, S. (1989) *Biochemistry* **28,** 7913–7918.
17. Amor-Gueret, M. & Levi-Strauss, M. (1990) *Nucleic Acids Res.* **18,** 1646.
18. Lindskog, S., Engberg, P., Forsman, C., Ibrahim, S. A., Jonsson, B. H., Simonsson, I. & Tibell, L. (1984) *Ann. N.Y. Acad. Sci.* **429,** 62–75.
19. Silverman, D. N., Tu, C. K., Tanhauser, S. M., Kresge, A. J. & Laipis, P. J. (1993) *Biochemistry* **32,** 10757–10762.
20. Okuyama, T., Sato, S., Zhu, X. L., Waheed, A. & Sly, W. S. (1992) *Proc. Natl. Acad. Sci. USA* **89,** 1315–1319.
21. Kabsch, W. (1993) *J. Appl. Crystallogr.* **26,** 795–800.
22. Nyborg, J. & Wonacott, A. J. (1977) in *The Rotation Method in Crystallography*, eds. Arndt, U. W. & Wonacott, A. J. (North-Holland, Amsterdam), pp. 139–152.
23. Navaza, J. (1994) *Acta Crystallogr.* **A50,** 157–163.
24. Collaborative Computing Project, Number 4 (1994) *Acta Crystallogr.* **D50,** 760–763.
25. Håkansson, K., Carlsson, M., Svensson, L. A. & Liljas, A. (1992) *J. Mol. Biol.* **227,** 1192–1204.
26. Bernstein, F. C., Koetzle, T. F., Williams, G. J. B., Meyer, E. F., Brice, M. D., Rodgers, J. R., Kennard, O., Shimanouchi, T. & Tasumi, M. (1977) *J. Mol. Biol.* **112,** 535–542.
27. Brünger, A. T., Kuriyan, J. & Karplus, M. (1987) *Science* **235,** 458–460.
28. Sack, J. S. (1988) *J. Mol. Graphics* **6,** 224–225.
29. Brünger, A. T. (1990) *Acta. Crystallogr.* **A46,** 46–57.
30. Brünger, A. T. (1992) *Nature (London)* **355,** 472–475.
31. Hewett-Emmett, D., Cook, R. G. & Dodgson, S. J. (1986) *Isozyme Bull.* **19,** 13.
32. Luzzati, P. V. (1952) *Acta Crystallogr.* **5,** 802–810.
33. Chothia, C. & Lesk, A. M. (1986) *EMBO J.* **5,** 823–826.
34. Christianson, D. W. & Alexander, R. S. (1989) *J. Am. Chem. Soc.* **111,** 6412–6419.
35. Lindskog, S. (1986) in *Zinc Enzymes*, eds. Bertini, I., Luchinat, C., Maret, W. & Zeppezauer, M. (Birkhauser, Boston), pp. 307–316.
36. Eriksson, A. E., Jones, T. A. & Liljas, A. (1988) *Protein Struct. Funct. Genet.* **4,** 274–282.
37. Krebs, J. F., Rana, F., Dluhy, R. A. & Fierke, C. A. (1993) *Biochemistry* **32,** 4496–4505.
38. Nair, S. K., Ludwig, P. A. & Christianson, D. W. (1994) *J. Am. Chem. Soc.* **116,** 3659–3660.
39. Nicholls, A. (1993) *GRASP: Graphical Representation and Analysis of Surface Properties* (Columbia Univ. Press, New York).
40. Vidgren, J., Liljas, A. & Walker, N. P. C. (1990) *Int. J. Biol. Macromol.* **12,** 342–344.
41. Burbaum, J. J., Ohlmeyer, M. H., Reader, J. C., Henderson, I., Dillard, L. W., Li, G., Randle, T. L., Sigal, N. H., Chelsky, D. & Baldwin, J. J. (1995) *Proc. Natl. Acad. Sci. USA* **92,** 6027–6031.
42. Whitney, P. L. & Briggle, T. V. (1982) *J. Biol. Chem.* **257,** 12056–12059.
43. Balboni, E. & Lehninger, A. L. (1986) *J. Biol. Chem.* **261,** 3563–3570.
44. Tannen, R. L. & Ross, B. D. (1983) *J. Lab. Clin. Med.* **102,** 536–542.
45. Dodgson, S. J. & Cherian, K. (1989) *Am. J. Physiol.* **257,** E791–E796.